



RESEARCH LETTER

10.1002/2016GL071537

Key Points:

- A coordinated air-sea sampling paradigm for targeting flow features and quantifying their kinematics over a range of scales is presented
- In situ observations of divergence and vorticity associated with fronts and eddies give mean values that can exceed $5f$
- Observed kinematic properties imply strong vertical velocities $O(10)$ m/h that can significantly influence biogeochemistry

Correspondence to:

J. C. Ohlmann,
carter@eri.ucsb.edu

Citation:

Ohlmann, J. C., M. J. Molemaker, B. Baschek, B. Holt, G. Marmorino, and G. Smith (2017), Drifter observations of submesoscale flow kinematics in the coastal ocean, *Geophys. Res. Lett.*, *44*, 330–337, doi:10.1002/2016GL071537.

Received 26 SEP 2016

Accepted 16 DEC 2016

Accepted article online 21 DEC 2016

Published online 13 JAN 2017

Drifter observations of submesoscale flow kinematics in the coastal ocean

J. C. Ohlmann¹ , M. J. Molemaker², B. Baschek^{3,4}, B. Holt⁵ , G. Marmorino⁶, and G. Smith⁶ 

¹Earth Research Institute, University of California, Santa Barbara, California, USA, ²Institute for Geophysics and Planetary Physics, University of California, Los Angeles, California, USA, ³Department of Atmospheric and Oceanic Sciences, University of California, Los Angeles, California, USA, ⁴Now at Institute of Coastal Research, Helmholtz-Zentrum Geesthacht, Geesthacht, Germany, ⁵Jet Propulsion Laboratory, California Institute of Technology, Pasadena, California, USA, ⁶Naval Research Laboratory, Washington, DC, USA

Abstract Fronts and eddies identified with aerial guidance are seeded with drifters to quantify submesoscale flow kinematics. The Lagrangian observations show mean divergence and vorticity values that can exceed 5 times the Coriolis frequency. Values are the largest observed in the field to date and represent an extreme departure from geostrophic dynamics. The study also quantifies errors and biases associated with Lagrangian observations of the underlying velocity strain tensor. The greatest error results from undersampling, even with a large number of drifters. A significant bias comes from inhomogeneous sampling of convergent regions that accumulate drifters within a few hours of deployment. The study demonstrates a Lagrangian sampling paradigm for targeted submesoscale structures over a broad range of scales and presents flow kinematic values associated with vertical velocities $O(10)$ m h⁻¹ that can have profound implications on ocean biogeochemistry.

1. Introduction

Ocean submesoscale turbulence is ubiquitous at length scales ranging from 10 m to 10 km and plays a critical role in surface layer mixing [Capet *et al.*, 2008a; McWilliams, 2016]. Submesoscale flows are characterized by large Rossby number, $Ro = \zeta/f$, where ζ is the relative vertical vorticity and f is the local planetary vorticity. When Ro is $O(1)$ or larger, lateral shear is equally important as, or stronger than, f and a breakdown of the geostrophic balance occurs. A transition between quasi two-dimensional and fully three-dimensional turbulence takes place, and the resulting forward energy cascade provides a means to dissipate larger-scale energy [McWilliams *et al.*, 2001; Muller *et al.*, 2005; Molemaker *et al.*, 2010]. Additionally, submesoscale motions in the surface layer are characterized by relatively large vertical velocities that can significantly influence ocean biogeochemistry by bringing nutrients into the euphotic zone and removing carbon from the upper ocean [Calil and Richards, 2010; Lévy *et al.*, 2012].

The distribution of ζ is expected to be asymmetric and skewed toward positive values when $Ro = O(1)$ (or larger [e.g., Hoskins and Bretherton, 1972; Rudnick, 2001]). The positively skewed asymmetry is found in high-resolution numerical simulations whenever submesoscale flows are not overshadowed by mesoscale eddies [Capet *et al.*, 2008a; Gula *et al.*, 2015]. Numerical studies suggest that submesoscale dynamics will ultimately dominate when scales become sufficiently small.

Despite the importance and presumed ubiquity of submesoscale turbulence, extreme observational challenges associated with flows that quickly evolve in time and space severely limit measurements of large Ro dynamics. Flows at scales between 10 and 100 km have been successfully diagnosed with a variety of observations. Lagrangian particle trajectories computed from remotely sensed satellite altimetry maps have been analyzed [e.g., Lehahn *et al.*, 2007; d'Ovidio *et al.*, 2009]. Shipboard hydrographic data from profiling and/or towed instruments have been used to investigate dynamic balances through inversion of the omega equation [e.g., Rudnick, 1996; Shearman *et al.*, 1999; Mahadevan and Tandon, 2006]. At these larger scales, Rossby numbers are relatively small, and departures from geostrophic balance are equally modest. The most successful observations of submesoscale dynamics occur on a 1 km scale with underway velocity profile data collected synchronously aboard two ships moving along parallel tracks [Shcherbina *et al.*, 2013]. In contrast to previous work, the parallel ship observations indicate flows with $Ro \sim O(1)$ and a marked asymmetry in the distribution of ζ skewed toward positive values.

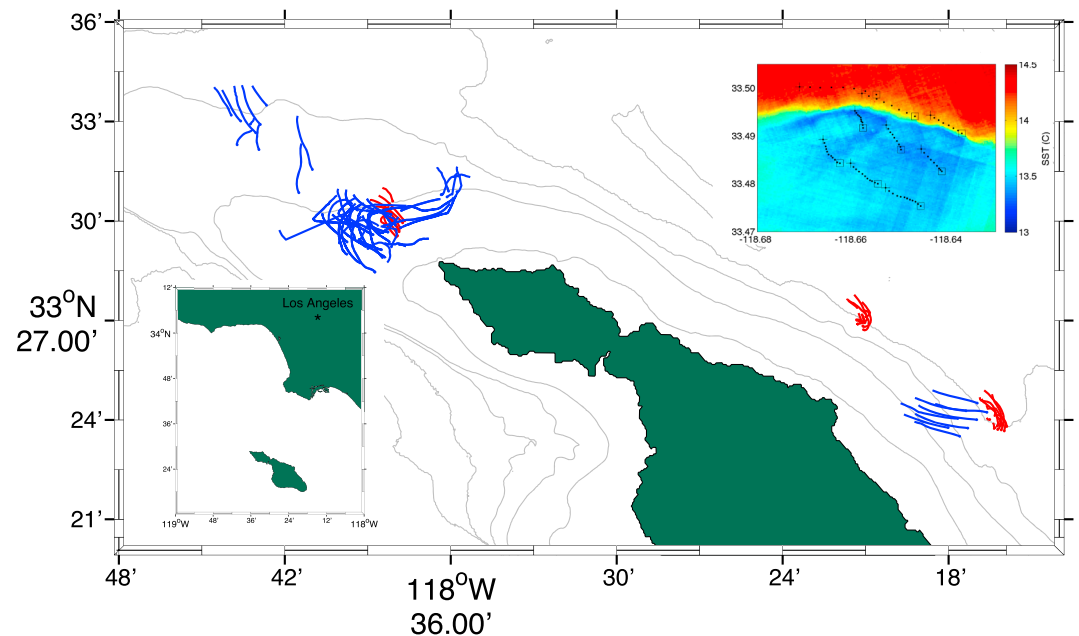


Figure 1. Drifter tracks recorded off the West End of Catalina Island in the Southern California Bight. Bathymetry contours shown every 200 m from 100 to 900 m. The squares indicate starting locations. Both temperature fronts (blue tracks) and eddies (red tracks) were targeted for sampling. The lower left inset map shows the location of Catalina Island relative to the Southern California coast. The upper right inset map shows drifter positions every 10 min (black dots; squares and crosses at starting and ending positions) overlaid on contemporaneous SST imagery from aircraft for a single deployment.

Drifter clusters provide an ideal sampling strategy for directly observing the ocean's quickly evolving structure. Drifters move with the flows they sample and thus record flows specific to submesoscale features while the features themselves are advected by larger-scale circulation. Drifter clusters also allow multiple spatial scales to be addressed in concert. By comparison, Eulerian observations from moorings only record flows associated with submesoscale features when the features are moving over the moorings. Single-ship surveys suffer from being too slow to resolve quickly varying spatial gradients in the velocity field. Two-ship surveys can overcome this but remain restricted to a single separation scale [Shcherbina *et al.*, 2013]. Despite the power of Lagrangian observations for diagnosing the submesoscale, the approach exists for relatively large scales [e.g., Paduan and Niiler, 1990; Swenson and Niiler, 1996; LaCasce and Ohlmann, 2003; Mariano *et al.*, 2016]. The advent of GPS-drifters allows historically large position errors to be overcome so smaller scales can now be resolved [Ohlmann *et al.*, 2005; Haza *et al.*, 2014]. What follows is a description of flow kinematics associated with submesoscale flow structures on scales ranging from 200 m to 4 km and 10 min to a few hours. The study also quantifies errors and sampling biases that must be considered when computing strain tensors from Lagrangian observations.

2. Data and Methods

2.1. Experimental Design

The experiment was designed to make in situ observations of specific submesoscale features identified with remotely sensed sea surface temperature (SST). The observations focus on flows associated with fronts and eddies near the west end of Catalina Island, located roughly 30 km off the Southern California coast (Figure 1). The location was chosen for its nearly constant submesoscale activity as identified in satellite and regional aircraft surveys [i.e., DiGiacomo and Holt, 2001; Marmorino *et al.*, 2010]. In situ sampling occurred during 3 days from 11 to 15 April 2011, and again during 6 days from 30 January to 6 February 2013. Sampling was performed during the winter-spring period when a relatively deep ocean mixed layer contains the greatest potential energy with which to force submesoscale motions [Fox-Kemper *et al.*, 2008].

Drifter clusters were deployed in a 3×3 square grid configuration with 1 km spacing over targeted submesoscale features identified with contemporaneous SST imagery recorded from aircraft (Figure 1). Drifters were deployed in the morning and retrieved at the end of the day (or occasionally when the targeted feature was no longer evident in aerial observations). The number of drifters was chosen to be as large as possible while still being manageable with a single boat. Microstar drifters, manufactured by Pacific Gyre Corporation (Oceanside, CA) specifically for use in coastal regions, were used [Ohlmann *et al.*, 2005]. The drifters record their position every 10 min by using GPS and transmit their data using the Iridium communications system. Data processing involves interpolating to a regular time grid with exact 10 min spacing and computing velocities as centered differences in position.

2.2. Differential Kinematic Property Calculations

A primary goal of the drifter deployments is observations from which horizontal surface velocity strain tensors can be computed and the differential kinematic properties (DKP) of the observed submesoscale structures characterized. The strain tensor comes from linear spatial gradients of the observed velocity field. A drifter cluster must have at minimum three units to compute velocity gradients in two dimensions. If the number of drifters is larger than three, a linear least squares approach that minimizes the eddy kinetic energy of the observations is used. Computation of the velocity strain tensor and associated DKP from clusters of drifters is presented in detail by Molinari and Kirwan [1975] and Okubo and Ebbesmeyer [1976].

As subsequently discussed, DKP calculations can become difficult to interpret as the directional separation in length scale over which velocity gradients are computed increases. In the limit, drifters in a cluster become aligned and gradients can only be computed in a single dimension. To account for the scale separation, a drifter cluster aspect ratio, α , is defined as

$$\alpha = \frac{L_{\text{minor}}}{L_{\text{major}}} \quad (1)$$

where L_{major} is the maximum distance between drifters within a cluster and L_{minor} is the maximum distance between drifters in the direction orthogonal to the L_{major} direction.

To compute DKP, all possible four-drifter clusters are identified for each nine-drifter deployment. Strain tensors are then calculated for each four-drifter combination at every 10 min time step as described above. Associated length scale ($L = (L_{\text{major}} + L_{\text{minor}})/2$) and α values are also computed. DKP statistics from combinations of the velocity strain tensor components are determined separately from observations associated with fronts (3 days) and eddies (6 days). Statistics are binned in 0.25 km L intervals, a width chosen to give a significant number of observations within each bin.

2.3. Observational Error Estimates

Errors in strain and DKP calculations can result from GPS positioning error and from observations that under-resolve the true flow field. GPS position error for the drifters used in this study (2–3 m) equates to a velocity error $O(0.5) \text{ cm s}^{-1}$ for the 10 min sampling interval [Ohlmann *et al.*, 2005]. A more significant source of error results from the fact that a finite set of point measurements generally undersamples the energy containing scales of the ocean's surface velocity field. The amount of sub-cluster-scale energy depends on the kinetic energy spectrum of the velocities and L of the sampling cluster. Least squares residuals from fits to the nine-drifter clusters [Okubo and Ebbesmeyer, 1976] give a mean error of 4 cm s^{-1} , consistent with the value for $L = 2 \text{ km}$ in a nearby location (also 4 cm s^{-1} [Ohlmann *et al.*, 2007]).

Propagation of the observational error in DKP calculations is quantified by Monte Carlo simulations, where drifter positions are perturbed with randomly generated noise drawn from a normal distribution with zero mean and 24 m standard deviation, σ . The position σ results from the 10 min sampling interval combined with a 4 cm s^{-1} standard deviation in velocity. Randomly placed virtual drifter clusters with m units are constructed and rescaled to $L = 2 \text{ km}$. Perturbation calculations are then performed for the randomly selected distributions of m -drifter clusters over the complete range of α . Probability density functions from the perturbations for computed values of δ and ζ as a function of drifter cluster size and α ultimately arise. Errors are quantified with the standard deviation, σ , of each distribution.

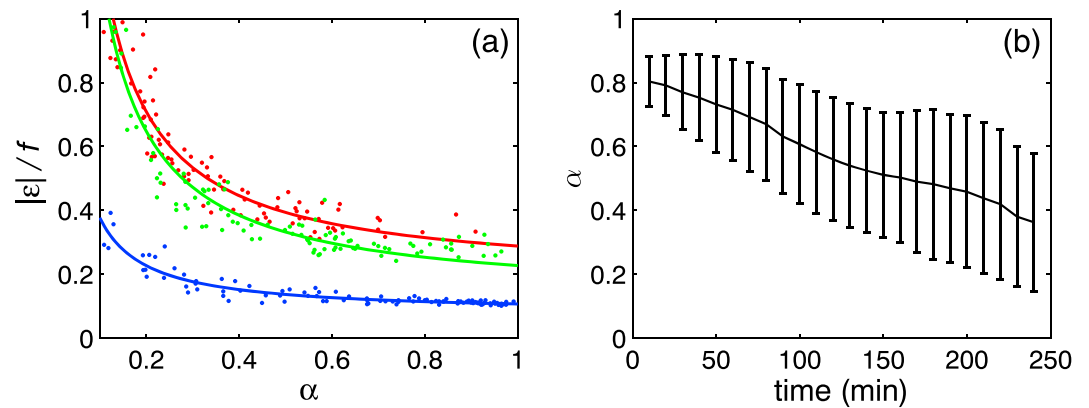


Figure 2. (left) Divergence error as a function of drifter cluster aspect ratio, α , from Monte Carlo simulations. The red, green, and blue colors correspond to results for clusters with 4, 9, and 100 drifters, respectively. (right) Time evolution of mean α for observed drifter clusters beginning with $\alpha > 0.7$. The vertical bars show the ± 1 standard deviation (σ) range. Values computed separately for drifter clusters sampling fronts and eddies both decrease linearly and are not qualitatively different; mean α values for the front clusters fall within the 1σ error bars for the eddy values and visa versa.

3. Results

3.1. Sampling Error and Drifter Cluster Aspect Ratio

Aspect ratio of a drifter cluster is the most significant factor in error estimation for δ and ζ . This makes sense considering that a fully two-dimensional strain field cannot be obtained with drifters aligned in a purely colinear manner [e.g., Righi and Strub, 2001]. The relationship between α and σ from the Monte Carlo error simulations for δ computed from four-drifter clusters shows $\sigma = 0.3f$ for $\alpha = 1$ (Figure 2a). Values of σ begin to increase dramatically to $\sigma > 0.5f$ for $\alpha < 0.3$. Results for nine-drifter clusters show a slight reduction in error as the extra drifters resolve more of the velocity field. It takes a large number of drifters ($O(100)$) to make dramatic decreases in σ .

The important result from the error analysis is that curves fit to σ scale as α^{-1} (Figure 2a). While there is some spread around the curve fits resulting from different spatial distributions of drifters, α of the cluster clearly dominates the error in the observed velocity strain field. Using more drifters reduces the error, but the reduction between clusters with four and nine drifters, the range of options available with the observations, is minor. Error calculations show that the expected error for a single determination of δ or ζ grows rapidly beyond $0.6f$ for $\alpha < 0.2$. Based on this result, error associated with DKP values in this study is constrained by excluding observations when $\alpha < 0.2$.

3.2. Sampling Bias and Time Dependence of Drifter Aspect Ratio

The time it takes the flow to deform drifter clusters from nearly square to a configuration with large α is order hours. On average, the four-drifter clusters that begin in a nearly square configuration reach $\alpha = 0.36$ after just 4 h (Figure 2b). The reduction in α with time is roughly linear and σ values are large, occasionally exceeding 0.20. Considering the mean minus one σ , 16% of drifter clusters have $\alpha < 0.2$ after 4 h from deployment. These clusters are expected to produce δ and ζ values with error bars approaching $1f$ (Figure 2a).

The quick deformation of drifter clusters can be driven by a variety of strain fields that may or may not be divergent. Divergent strain fields promote a sampling bias with more drifters in regions of negative δ rather than positive δ . The bias is expected to increase with sampling time as the flow field continually redistributes drifters toward negative δ zones. The distribution of δ from drifter clusters sampling fronts immediately after deployment on a square grid is representative of a normal distribution (Figure 3a, blue curve). The δ distribution after 4 h becomes bimodal with a large peak at $-2f$ and a smaller peak between $\pm 1f$ (Figure 3a, red curve). The change in δ distribution with time demonstrates a divergent flow field and a bias toward sampling negative δ . Similarly, the distribution of δ from drifter clusters sampling eddies shifts from being positively skewed (Figure 3b, blue curve) to being centered about zero (Figure 3b, red curve). This is consistent with eddies showing positive δ (discussed below) and an associated bias toward undersampling positive δ regions. To account for these biases, only drifter observations within 4 h of deployment are used for computing DKP statistics.

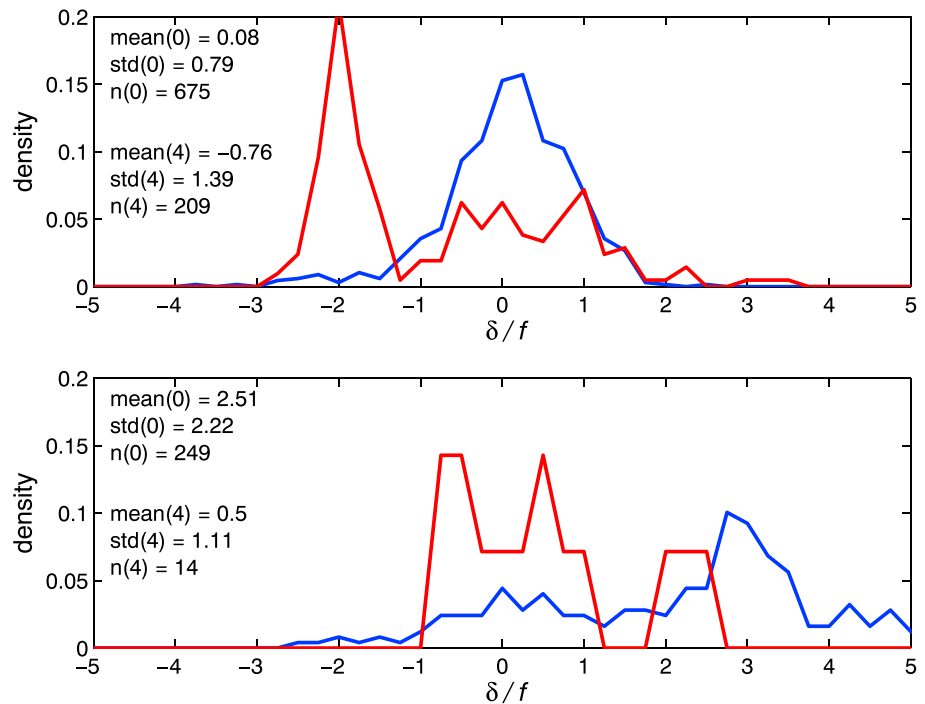


Figure 3. Distributions of divergence just after drifter deployment in square grids (blue curves) and after 4 h of sampling (red curves) for drifters sampling (top) fronts and (bottom) eddies. The mean, standard deviation, and sample size of each distribution in a panel are quantified.

3.3. Divergence and Vorticity Distributions

The primary results relating to ocean dynamics come from DKP distributions (Figure 4). Mean δ and ζ values on scales ranging from 0.25 to 4 km can be many times f with significant variation. The distributions computed from drifter clusters sampling fronts show (on average) negative δ and positive ζ as expected (mean $\delta = -0.1f$ and $\zeta = 0.7f$; Figures 4a and 4b). The distributions computed from drifter clusters sampling eddies are quite different. The eddy clusters give (on average) much larger positive ζ and significant positive δ . Mean values of δ and ζ from eddy clusters are $2.3f$ and $5.4f$, respectively (Figures 4c and 4d). These values are the largest observed to date, many times larger than observed in the Gulf Stream region for a length scale of 1 km [Shcherbina *et al.*, 2013].

The least squares approach for determining δ and ζ from a drifter cluster effectively amounts to a filtering of the strain field at the length scale of the cluster. Length-scale dependence of mean square DKP variables ($\langle \delta^2 \rangle$, $\langle \zeta^2 \rangle$) shows a significant increase in flow field variance with decreased filter scale (Figure 5). This result arises simply from an accumulation of variance with each additional scale. The increase in variance with decreased filter scale is equal to the amount of variance at the added scale (Figure 5). The significant mean slopes of the $\langle \delta^2 \rangle$ and $\langle \zeta^2 \rangle$ curves are thus indicative of a relatively flat variance spectrum as variance continues to be accumulated with decreased length scale. Theoretically, the curves should be monotonically decreasing, as variance is a positive definite quantity. The noise in the curves is the result of inhomogeneous sampling by Lagrangian drifters. The scale-dependent $\langle \delta^2 \rangle$ and $\langle \zeta^2 \rangle$ values presented are consistent with values at similar scales observed with just a few observations in the Kuroshio region suggesting universal behavior [Kawai, 1985].

4. Discussion

4.1. Error Estimates, Sampling Bias, and DKP Calculations

Clusters of four drifters are chosen for DKP calculations to maximize the number of unique combinations from each set of nine drifters (126), and thus the number of values used for computing statistics. (Each cluster of nine drifters that samples every 10 min for 4 h yields 3024 separate strain tensors.) Computing fits for each individual four-drifter cluster allows a wider range of L to be isolated compared with fits to nine-drifter clusters. Clusters of at

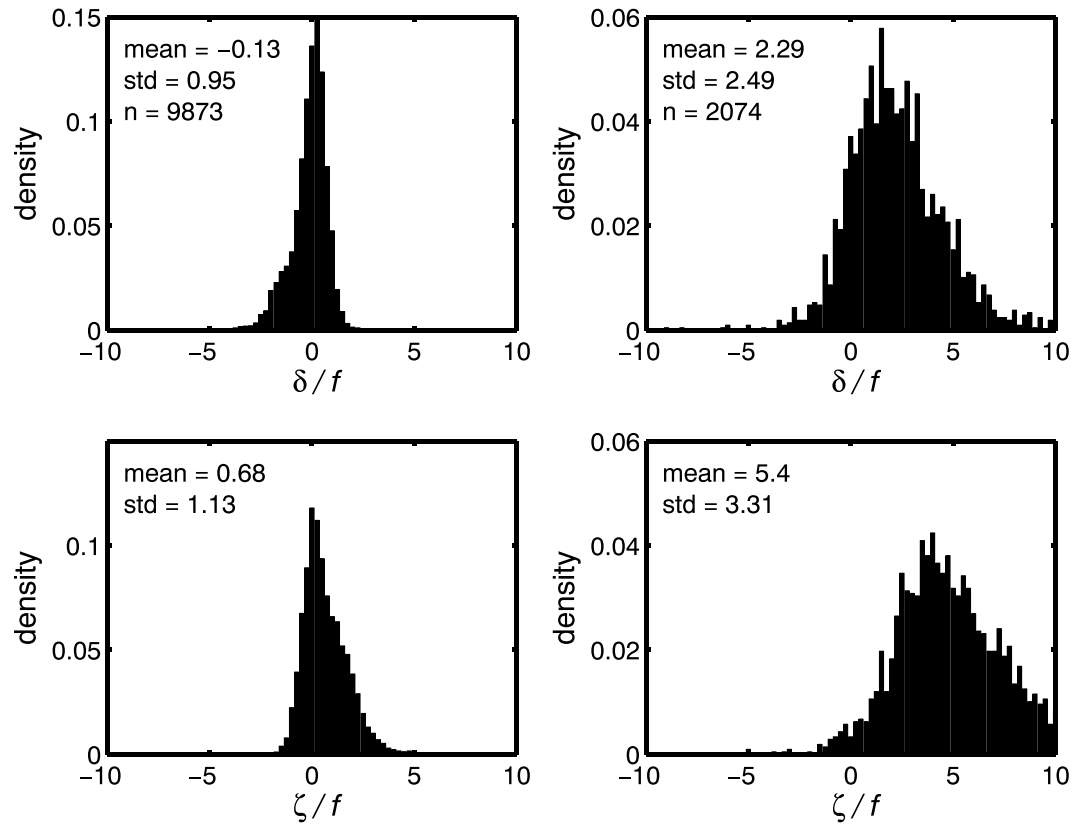


Figure 4. Histograms of (top row) divergence and (bottom row) vorticity values from four-drifter polygons located over (left column) fronts and (right column) eddies sampling length scales between 0.3 and 4.0 km. Bins are $0.25f$ in width. Values in each bin normalized by the total number of observations.

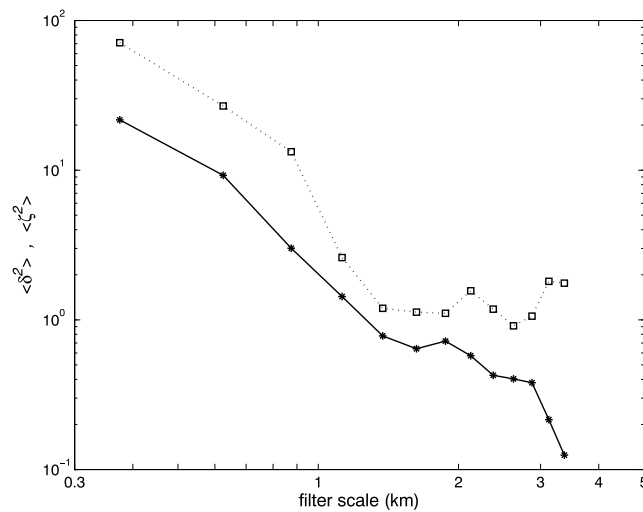


Figure 5. RMS divergence (solid line) and vorticity (dashed line) as a function of length scale. Values are from DKP calculations using all available four-drifter clusters with aspect ratio of >0.2 and shown in units of f . Values are shown as bin averages for 0.25 km wide bins between 0.25 and 3.5 km. The number of observations in each bin ranges from 70 (0.25–0.5 km bin) to 2190 (1.75 to 2.0 km bin).

least six drifters are suggested for meaningful confidence limits on residual vorticities [Okubo and Ebbesmeyer, 1976]. This study is focused on error in DKP statistics, not residual velocities. The Monte Carlo simulations do not indicate an appreciable decrease in error as the number of drifters in a cluster increases from 4 to 9.

Although error can be quantified with residuals from the least squares fits, a Monte Carlo approach is chosen. The Monte Carlo approach allows error to be computed for drifter cluster sizes and α values beyond those available from observations (i.e. Figure 2a). In addition, the Monte Carlo analysis does not impose assumption of uncorrelated turbulent fluctuations and measurement errors. Mean error in the observed drifter configurations from the least squares residuals is 4 cm s^{-1} , which is equivalent to the value used in the Monte Carlo analysis.

Drifter clusters are truly independent only if drifters in a specific cluster are not used in any other cluster. Only two truly independent four-drifter clusters can be formed from each nine-drifter deployment. Decorrelation time scales for residual drifter velocities are near 30 min (not shown). Thus, each nine-drifter cluster that samples for 4 h yields a maximum of 16 truly independent observations. The independence criterion for Lagrangian observations is typically relaxed to maximize the generally limited number of samples. Despite statistics from thousands of observations, the true number of degrees of freedom for the front and eddy observations is 112 and 48. DKP statistics from truly independent observations are not qualitatively different from the case where unique four-drifter clusters are chosen from nine-drifter sets with replacement. Clusters that form into a desired configuration through chance distortion by the flow [e.g., *LaCasce and Ohlmann, 2003; LaCasce, 2008*] are biased and are not included here.

Results indicate that drifter observations can become biased by the flows they sample after just a few hours (Figures 2b and 3). In areas of intense submesoscale energy, drifters deployed on a regularly spaced grid will tend to move from areas of divergence to become aligned in convergent features; thereafter, the drifters trace out the larger-scale advection of those features, rather than continuing to provide data on smaller-scale differential properties of the flow field. Unbiased Lagrangian sampling at the scales considered here should be limited to observations within the first few hours of deployment. For robust statistics, this requires multiple deployments of a relatively small number of drifters or a single deployment of a much larger grid. A single deployment of near 80 drifters is necessary to obtain a similar number of degrees of freedom as obtained in this study through repetitive deployment of just nine drifters.

4.2. Submesoscale Dynamics

Drifter observations and associated DKP are from targeted submesoscale structures in the coastal region that are presumably generated by the interaction of the flow with bathymetry [*Signell and Geyer, 1991; Dong and McWilliams, 2007*]. Distributions of δ and ζ values from observations collected with two side-by-side ships (with 1 km separation [*Shcherbina et al., 2013*]) covering 500 km in the North Atlantic show values of $O(1) f$, with mean values near zero. Numerous factors can explain the larger values found in this study: observations are (1) from a coastal region where bathymetry is expected to promote shear, (2) from targeted flow features expected to have significant strain fields, and (3) extended to scales even smaller than 1 km.

The negative δ and positive ζ values associated with observed temperature fronts are consistent with frontal dynamics theory and relate to the conservation of potential vorticity [*Capet et al., 2008b; Gula et al., 2015; McWilliams et al., 2009, 2015*]. They can be associated with pronounced vertical velocities and thus considerably more nutrient exchange and export production for ocean biogeochemistry than previously identified [*Klein and Lapeyre, 2009; Lévy et al., 2012*]. Based on the continuity equation, δ and ζ values of $3f$, combined with an upper ocean mixed layer depth $O(20)$ m as observed, give vertical velocities $O(10) \text{ m h}^{-1}$.

Observations of positive δ and ζ values associated with eddies are not as easily interpreted. In general, the regional circulation suggests a coastal boundary layer with positive ζ during northwestward flows [*Dong and McWilliams, 2007*]. Instabilities of this boundary layer may lead to the formation of cyclonic eddies with large positive ζ as observed. While the observations of positive ζ are not surprising, the coincident observations of significant positive δ are harder to explain. One possibility is that observations were collected during the time of transient geostrophic adjustment of the cyclonic flow. While upwelling is expected during the adjustment process, this is the first time such large positive δ values have been reported.

5. Conclusions and Summary

Presented here are Lagrangian observations of flow kinematics for specific fronts and eddies at scales of a few kilometers and less. The targeted scales and GPS drifter position accuracy make the drifter observations novel. Using this approach, significant departures from geostrophic flows are observed with average Rossby number, Ro , exceeding 5. These are the largest Ro values observed in situ to date. The divergence of surface velocities indicates pronounced vertical fluxes on the order of 10 m h^{-1} . This study demonstrates a reliable sampling paradigm that can be applied to *the entire range of scales* within the submesoscale. Determining how best to target and measure submesoscale turbulence is an important first step toward understanding how ageostrophic flows within this scale range influence both the ocean energy budget and ocean biogeochemistry.

Acknowledgments

The authors wish to acknowledge the Southern California Marine Institute for use of their marine facilities. Discussions with Denny Kirwan and Baylor Fox-Kemper helped shape the study. The LAPCOD 2015 meeting facilitated these conversations. Support for this work comes from the National Aeronautics and Space Administration (NASA: SB110079), the National Oceanic and Atmospheric Administration (NOAA: NA10OAR4320156), and the Office of Naval Research (ONR: N000141210105, N00014141062, 72-9201 and 72-1C02). Data used in the study are available from the authors.

References

- Calil, P. H. R., and K. J. Richards (2010), Transient upwelling hot spots in the oligotrophic North Pacific, *J. Geophys. Res.*, *115*, C02003, doi:10.1029/2009JC005360.
- Capet, X., J. C. McWilliams, M. J. Molemaker, and A. Shchepetkin (2008a), The transition from mesoscale to submesoscale in the California Current System. Part I: Flow structure, eddy flux and observational tests, *J. Phys. Oceanogr.*, *38*, 29–43, doi:10.1017/jfm.2012.90.
- Capet, X., J. C. McWilliams, M. J. Molemaker, and A. Shchepetkin (2008b), The transition from mesoscale to submesoscale in the California Current System. Part II: Frontal processes, *J. Phys. Oceanogr.*, *38*, 44–64, doi:10.1175/2007JPO3672.1.
- DiGiacomo, P., and B. Holt (2001), Satellite observations of small coastal ocean eddies in the Southern California Bight, *J. Geophys. Res.*, *106*(C10), 22,521–22,543, doi:10.1029/2000JC000728.
- Dong, C., and J. McWilliams (2007), A numerical study of island wakes in Southern California Bight, *Cont. Shelf Res.*, *27*, 1233–1248, doi:10.1016/j.csr.2007.01.016.
- d'Ovidio, F., J. Isern-Fontanet, C. López, E. Hernández-García, and E. García-Ladona (2009), Comparison between Eulerian diagnostics and finite-size Lyapunov exponents computed from altimetry in the Algerian basin, *Deep Sea Res.*, *56*, 15–31, doi:10.1016/j.dsr.2008.07.014.
- Fox-Kemper, B., R. Ferrari, and R. W. Hallberg (2008), Parameterization of mixed layer eddies. Part I: Theory and diagnosis, *J. Phys. Oceanogr.*, *38*, 1145–1165, doi:10.1017/jfm.2015.700.
- Gula, J., M. J. Molemaker, and J. C. McWilliams (2015), Gulf stream dynamics along the southeastern U.S. seaboard, *J. Phys. Oceanogr.*, *45*, 690–715, doi:10.1175/JPO-D-14-0154.1.
- Haza, A. C., T. M. Özgökmen, A. Griffa, A. C. Poje, and M.-P. Lelong (2014), How does drifter position uncertainty affect ocean dispersion estimates?, *J. Atmos. Oceanic Tech.*, *31*, 2809–2828.
- Hoskins, B. J., and F. P. Bretherton (1972), Atmospheric frontogenesis models: Mathematical formulation and solution, *J. Atmos. Sci.*, *29*(1), 11–37, doi:10.1175/1520-0469.
- Kawai, H. (1985), Scale dependence of divergence and vorticity of near-surface flows in the sea: Part 2. Results and interpretation, *J. Oceanogr. Soc. Japan*, *41*, 167–179, doi:10.1007/BF02111116.
- Klein, P., and G. Lapeyre (2009), The oceanic vorticity pump induced by mesoscale and submesoscale turbulence, *Ann. Rev. Mar. Sci.*, *1*, 351–375, doi:10.1146/annurev.marine.010908.163704.
- LaCasce, J. H. (2008), Statistics from Lagrangian observations, *Prog. Oceanogr.*, *77*, 1–29, doi:10.1016/j.pocean.2008.02.002.
- LaCasce, J. H., and J. C. Ohlmann (2003), Relative dispersion at the surface of the Gulf of Mexico, *J. Mar. Res.*, *61*, 285–312, doi:10.1357/002224003322201205.
- Lehahn, Y., F. d'Ovidio, M. Lévy, and E. Heifetz (2007), Stirring of the northeast Atlantic spring bloom: A Lagrangian analysis based on multisatellite data, *J. Geophys. Res.*, *112*, C08005, doi:10.1029/2006JC003927.1.
- Lévy, M., R. Ferrari, P. J. S. Franks, A. P. Martin, and P. Rivière (2012), Bringing physics to life at the submesoscale, *Geophys. Res. Lett.*, *39*, L14602, doi:10.1029/2012GL052756.
- Mahadevan, A., and A. Tandon (2006), An analysis of mechanisms for submesoscale vertical motion at ocean fronts, *Ocean Model.*, *14*, 241–256, doi:10.1029/2008JC005203.
- Mariano, A. J., et al. (2016), Statistical properties of the surface velocity field in the northern Gulf of Mexico sampled by GLAD drifters, *J. Geophys. Res. Oceans*, *121*, 5193–5216, doi:10.1002/2015JC011569.
- Marmorino, G. O., B. Holt, M. J. Molemaker, P. M. DiGiacomo, and M. A. Sletten (2010), Airborne synthetic aperture radar observations of “spiral eddy” slick patterns in the Southern California Bight, *J. Geophys. Res.*, *115*, doi:10.1029/2009JC005863.
- McWilliams, J. C. (2016), Submesoscale currents in the ocean, *Proc. R. Soc. A*, *472*, 20160117, doi:10.1098/rspa.2016.0117.
- McWilliams, J. C., M. J. Molemaker, and I. Yavneh (2001), From stirring to mixing of momentum: Cascades from balanced flows to dissipation in the oceanic interior, in *Aha Huliko'a Proceedings: 2001* edited by, edited by P. Muller, pp. 59–66, U. Hawaii, Honolulu.
- McWilliams, J. C., F. Colas, and M. J. Molemaker (2009), Cold filamentary intensification and oceanic surface convergence lines, *Geophys. Res. Lett.*, *36*, L18602, doi:10.1029/2009GL039402.
- McWilliams, J. C., J. Gula, M. J. Molemaker, L. Renault, and A. F. Shchepetkin (2015), Filament frontogenesis by boundary layer turbulence, *J. Phys. Oceanogr.*, *45*, 1988–2005, doi:10.1175/JPO-D-14-0211.1.
- Molemaker, M. J., J. C. McWilliams, and X. Capet (2010), Balanced and unbalanced routes to dissipation in an equilibrated Eady flow, *J. Fluid Mech.*, *654*, 35–63, doi:10.1017/S0022112009993272.
- Molinari, R., and A. D. Kirwan (1975), Calculations of differential kinematic properties from Lagrangian observations in western Caribbean Sea, *J. Phys. Oceanogr.*, *5*, 483–491.
- Muller, P., J. McWilliams, and J. Molemaker (2005), Routes to dissipation in the ocean: the 2D/3D turbulence conundrum, in *Marine Turbulence: Theories, Observations and Models*, edited by H. Baumert, J. Simpson, and J. Sundermann, pp. 397–405, Cambridge Univ. Press, Cambridge.
- Ohlmann, C., P. White, L. Washburn, E. Terrill, B. Emery, and M. Otero (2007), Interpretation of coastal HF radar derived surface currents with high-resolution drifter data, *J. Atmos. Oceanic Tech.*, *24*, 666–680, doi:10.1175/.
- Ohlmann, J. C., P. F. White, A. L. Sybrandy, and P. P. Niiler (2005), GPS-cellular drifter technology for coastal ocean observing systems, *J. Atmos. Oceanic Tech.*, *22*, 1381–1388.
- Okubo, A., and C. C. Ebbesmeyer (1976), Determination of vorticity, divergence, and deformation rates from analysis of drogoue observations, *Deep-Sea Res.*, *23*, 349–352.
- Paduan, J. D., and P. P. Niiler (1990), A Lagrangian description of motion in Northern California coastal transition filaments, *J. Geophys. Res.*, *95*, 18,095–18,109, doi:10.1029/JC095iC10p18095.
- Righi, D. D., and T. Strub (2001), The use of simulated drifters to estimate vorticity, *J. Mar. Syst.*, *29*, 125–140.
- Rudnick, D. L. (1996), Intensive surveys of the Azores Front: 2. Inferring the geostrophic and vertical velocity fields, *J. Geophys. Res.*, *101*(C7), 16,291–16,303, doi:10.1029/96JC01144.
- Rudnick, D. L. (2001), On the skewness of vorticity in the upper ocean, *Geophys. Res. Lett.*, *28*(10), 2045–2048, doi:10.1029/2000GL012265.
- Shcherbina, A. Y., E. A. D'Asaro, C. M. Lee, J. M. Klymak, M. J. Molemaker, and J. C. McWilliams (2013), Statistics of vertical vorticity, divergence, and strain in a developed submesoscale turbulence field, *Geophys. Res. Lett.*, *40*, 4706–4711, doi:10.1002/grl.50919.
- Shearman, R. K., J. M. Barth, and P. M. Kosro (1999), Diagnosis of three-dimensional circulation associated with mesoscale motion in the California current, *J. Phys. Oceanogr.*, *29*, 651–670.
- Signell, R. P., and W. R. Geyer (1991), Transient eddy formation around headlands, *J. Geophys. Res.*, *96*(C2), 2561–2575, doi:10.1029/90JC02029.
- Swenson, M. S., and P. P. Niiler (1996), Statistical analysis of the surface circulation of the California Current, *J. Geophys. Res.*, *101*, 22,631–22,645, doi:10.1029/96JC02008.